



Optimal geometric characterization of forced zonal mean tropical precipitation changes

A. Donohoe¹ · A. R. Atwood² · D. S. Battisti³

Received: 7 July 2021 / Accepted: 9 February 2022

© The Author(s), under exclusive licence to Springer-Verlag GmbH Germany, part of Springer Nature 2022

Abstract

The zonal and annual mean tropical precipitation response to paleoclimate and anthropogenic forcing scenarios ranging from the Last Glacial Maximum (LGM), CO₂ quadrupling (4XCO₂), mid-Holocene, North Atlantic freshwater hosing and volcanic forcing is analyzed in an ensemble of global climate models. Zonally averaged tropical precipitation changes are characterized in terms of three geometric manipulations of the climatological precipitation (hereafter, modes): meridional shifts, intensifications, and meridional contractions. We employ an optimization procedure that quantifies the magnitude and robustness (across different models) of changes in each mode in response to each forcing type. Additionally, the fraction of precipitation changes that are explained by the modes—in isolation and combined—is quantified. Shifts are generally less than 1° latitude in magnitude and explain a small fraction (< 10%) of tropical precipitation changes. Contractions and intensifications are strongly correlated across all simulations with a robust intensification and contraction of precipitation under global warming and a robust reduction and expansion under global cooling during the Last Glacial Maximum. The near constant scaling between contractions and intensifications across all simulations is used to define a joint contraction/intensification (*CI*) mode of tropical precipitation. The *CI* mode explains nearly 50% of the precipitation change under 4XCO₂ and LGM forcing by optimizing a single parameter. These results suggest the shifting mode that has been extensively used to interpret paleo-rainfall reconstructions is of limited use for characterizing forced zonal mean precipitation changes and advocates for a reinterpretation of past precipitation changes to account for the *CI* mode.

Keywords Tropical precipitation · ITCZ · Paleoclimate · Tropical contraction

1 Introduction

The concept of a meridional shift of the intertropical convergence zone (ITCZ) is ubiquitous in both the paleoclimate and climate dynamics literature for describing spatial patterns of forced tropical precipitation changes. Here, we define an ITCZ shift as a meridional translation of the climatological tropical precipitation pattern. In paleoclimate studies, concurrent increases and decreases of precipitation in different latitude bands within the tropics have commonly

been interpreted as a meridional translation (shift) of the ITCZ including: (1) southward ITCZ shifts in response to Heinrich events (Jacobel et al. 2016; Wang et al. 2001) characterized by North Atlantic iceberg discharge; (2) southward ITCZ shifts during the Little Ice Age (Pahnke et al. 2007; Haug et al. 2001; Sachs et al. 2009) when proxy evidence suggests the Northern Hemisphere was cold relative to the Holocene; (3) northward ITCZ shifts during the early Holocene (Haug et al. 2001; Bird et al. 2011; Wang et al. 2001; Sachs et al. 2018) when precessional phasing intensified boreal summer insolation; and (4) southward ITCZ shifts during the Last Glacial Maximum (Arbuszewski et al. 2013; Koutavas and Lynch-Stieglitz 2004) when large ice sheets occupied the Northern Hemisphere continents. A meridional translation of a strongly peaked climatological precipitation distribution would result in a dipole of precipitation anomalies. Thus, the contrasting precipitation changes across different latitude bands discerned from compilations

✉ A. Donohoe
adonohoe@u.washington.edu

¹ Polar Science Center, Applied Physics Laboratory,
University of Washington, Seattle, WA 98195, USA

² Department of Earth Ocean and Atmospheric Science,
Florida State University, Tallahassee, USA

³ Department of Atmospheric Sciences, University
of Washington, Seattle, USA

of paleoclimate records are qualitatively consistent with an ITCZ shift (Arbuszewski et al. 2013; Sachs et al. 2009).

In idealized dynamical studies (i.e. aquaplanet simulations) forced by hemispherically asymmetric heating/cooling, the ITCZ very clearly shifts towards the hemisphere in which the atmosphere is heated more strongly. This ITCZ response is commonly understood in terms of the Hadley cell shifting in order to redistribute the excess energy in the warmed hemisphere to the opposite hemisphere (Kang et al. 2008; Wei and Bordoni 2018; Frierson and Hwang 2012). The same zonal mean ITCZ shift in response to hemispherically asymmetric forcing is also seen in comprehensive coupled climate models (Chiang and Bitz 2005; Schneider et al. 2014; Kang 2020). However, the spatial pattern of forced precipitation changes in models with zonal asymmetries such as geography, ocean circulations and a seasonal cycle is more complicated than a simple shift of the climatological precipitation pattern. ITCZ shifts in comprehensive models are diagnosed in a myriad of ways, including changes in the “precipitation centroid” (P_{CENT} which is akin to a gravitational center of mass Frierson and Hwang 2012), the hemispheric difference in tropical precipitation (Hwang et al. 2013), the precipitation power-weighted latitude or “moment” (Adam et al. 2016a), or by simply noting the spatial map of precipitation change is characterized by a meridional dipole. These various ITCZ shift metrics have different strengths and weaknesses, but in nearly all cases, little effort has been made to quantify how much of the forced precipitation changes can be explained by an ITCZ shift.

Consider the following example of how a tropical precipitation change that does not involve a meridional translation of precipitation might be misdiagnosed as an “ITCZ shift” starting from a climatological tropical precipitation distribution that is bi-modal with peaks north and south of the equator—as is common in many climate model simulations (e.g. the black line in Fig. 1A). Assume that, in response to external forcing, the precipitation peak in the NH is intensified with no other changes in the distribution. This precipitation change would be diagnosed as “northward shift” in the common metrics used in the literature (e.g. P_{CENT} , precipitation weighted moments, hemispheric contrast of precipitation). However, a meridional translation of the climatological precipitation is a poor characterization of the precipitation change since the locations of the tropical precipitation peaks have not moved. Adam (2021) and Zhao and Federov (2020) recently demonstrated that the tropical precipitation changes in idealized and comprehensive model settings are better characterized by pulsing of the peaks rather than meridional translations for states that have bi-modal tropical precipitation peaks.

In this manuscript, we quantify how well a meridional shift in the climatological zonal mean precipitation pattern characterizes simulated precipitation changes (ΔP) under a

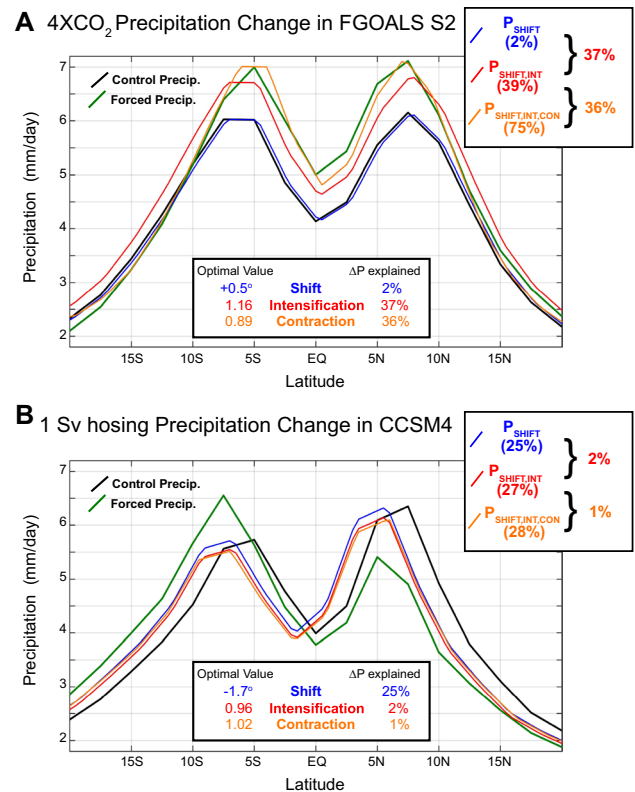


Fig. 1 Illustration of optimal fitting to shifted/contracted/intensified modes of tropical precipitation and the procedure used to define the percent of the precipitation change explained by each mode. The black line shows the climatological (zonal and annual mean) precipitation in the control (pre-industrial) simulations and the green line shows the precipitation after external forcing. First the precipitation is optimally shifted (P_{SHIFT} , blue line). Next the precipitation is optimally intensified and shifted together ($P_{SHIFT,INT}$, red line). Finally, the precipitation is optimally contracted, intensified and shifted together ($P_{SHIFT,INT,CON}$, orange line). The percentage of ΔP explained by each mode is defined as the additional reduction in (normalized) RMS ΔP by successively introducing the mode and all optimal parameters are defined from optimizing the three modes simultaneously. Panel **A** shows an example of a 4XCO₂ precipitation response that is well described by a intensification and contraction. Panel **B** shows the precipitation response to freshwater hosing that is best described by a southward shift

myriad of climate forcings in the following way. The climatological zonal mean tropical precipitation distribution is shifted north and south in search of the resultant pattern that best matches the simulated precipitation in response to forcing; the fraction of ΔP explained by the shift is quantified by how well the optimally shifted distribution matches the forced response. This procedure also provides a new metric for quantifying the magnitude of ITCZ shifts (optimized value of the translation in degrees latitude) that can be compared against other commonly used metrics to address how far the ITCZ shifts in model simulations. Additionally, we ask if there are other geometric manipulations of the climatological precipitation (hereafter, modes) that explain

a larger fraction of simulated tropical precipitation changes than the shifting mode. Specifically we analyze two additional modes: (1) intensification of the precipitation distribution with no change in shape and (2) meridional contraction/expansion of the precipitation distribution about the equator. These three modes—shifting, intensifying and contracting—are optimally fit, in conjunction, to best match the forced changes in precipitation.

We consider forced precipitation changes in large ensembles of climate models across a myriad of different climate forcings including: (1) CO₂ forcing; (2) Last Glacial Maximum orbital parameters and boundary conditions; (3ii) mid-Holocene orbital parameters and greenhouse gas concentrations; (4) freshwater hosing of the North Atlantic and (5) volcanic forcing. We limit our analyses to annual and zonal mean precipitation changes (hereafter ΔP) in the current manuscript, to focus on characterizing the modes of tropical precipitation changes on the broadest spatial-temporal scale while acknowledging that there are robust zonally-inhomogeneous and seasonal changes of tropical precipitation that are comparable in magnitude to the zonal, annual mean changes (Atwood et al. 2020; Donohoe et al. 2019; Haug et al. 2001; Yan et al. 2015; Braconnot et al. 2012; Liu et al. 2018).

This manuscript is organized as follows. The model simulations that we analyze and the methodology for optimally characterizing the tropical precipitation changes are described in Sect. 3. The resulting optimal characterization of ΔP in terms of shifts, intensifications, and contractions and the fraction of precipitation changes described by each mode across the different prescribed forcing scenarios are described in Sect. 4. A summary and discussion follows.

2 Model simulations analyzed and methodology

Here we describe the suite of coupled climate model simulations and forcing scenarios for which ΔP is analyzed and the methodology for optimally characterizing ΔP in terms of shifting, intensifying and contracting modes.

2.1 Model simulations analyzed

We make use of model output for idealized anthropogenic (abrupt CO₂ quadrupling) and paleoclimate (LGM, mid-Holocene, and last millennium) forcing scenarios run across an ensemble of different climate models as part of the Climate Model Inter-comparison Project (Taylor et al. 2012) and Paleoclimate Model Inter-comparison Project (Braconnot et al. 2007a, 2012). Additional volcanic and freshwater forcing simulations are analyzed in a subset of coupled climate models. Atwood et al. (2020) analyzed the zonal

structure of tropical precipitation changes in the same suite of model simulations investigated here and additional details of the simulations are provided there. All together, 95 sets of forced simulations and companion control simulations are analyzed in this study.

2.1.1 CO₂ quadrupling

22 simulations from the abrupt CO₂ quadrupling experiment (hereafter 4XCO₂) of CMIP5 (Taylor et al. 2012) are analyzed in which atmospheric CO₂ concentrations are instantly quadrupled relative to pre-industrial (PI) levels and held fixed thereafter. ΔP is evaluated from the difference between the climatology in years 100–150 after quadrupling in the 4XCO₂ simulations and that in the PI control simulation in the same model.

2.1.2 Last Glacial Maximum—LGM

13 total LGM simulations are analyzed with 7 from PMIP2 (Braconnot et al. 2007a) and 6 from PMIP3 (Braconnot et al. 2012). LGM simulations are forced by solar insolation from 21,000 years before present, greenhouse gas (CO₂, CH₄, N₂O) and aerosol concentrations are set based on ice core data (CO₂ is set to 185 ppm) coastlines are set to be consistent with a 120 m decrease in sea level, and the land ice topography is prescribed as specified in Kageyama et al. (2018) which includes the expansive Laurentide ice sheet over North America. ΔP is evaluated from the LGM climatology calculated from years 31 to 200 after a spin up period.

2.1.3 Mid Holocene

12 PIMP3 (Braconnot et al. 2012) mid-Holocene simulations are analyzed. Simulations are forced by orbital parameters representative of 6000 years before present from Berger (1978). Most significantly, due to orbital precession, the seasonal cycle of insolation in the Northern Hemisphere was amplified 6000 years ago while the duration of summer was reduced. We note that in the annual average the sum of all mid-Holocene forcing agents are symmetric about the equator.

2.1.4 Freshwater hosing

18 total simulations of North Atlantic freshwater forcing (aka ‘hosing’) are analyzed – 16 from the Community Climate System Model version 4 (CCSM4) as described in Atwood et al. (2020) and 1 each with Max Planck Institute of Meteorology OM1 model and the United Kingdom Hadley Center CM3 model as described in Timmermann et al. (2007). In each simulation either 1.0 Sv or 0.1 Sv of freshwater forcing is imposed across the surface of the North Atlantic Ocean (from 50 to 70° N) for 100 years. ΔP

is calculated from the climatology averaged over the last 80 years of simulation (it takes approximately 20 years for the Atlantic Meridional Overturning circulation to fully respond to the freshwater forcing). Four ensemble members were performed with the default configuration of CCSM4 with 1.0 Sv freshwater forcing. The same freshwater forcing was also applied to two biascorrected versions of the model. The bias corrections were: (1) a modification to the orography of Central America (which reduced the biases in the eastern Pacific climatology associated with the poor resolution of Central American topography; Baldwin et al. 2021) and (2) surface heat flux modifications with a cyclostationary seasonal cycle throughout the tropical oceans (30° S to 30° N) to further reduce the bias in the climatological seasonal cycle in SST. In one configuration of the model with three ensemble members and 1.0 Sv of freshwater forcing, only the Central American topography was modified with no changes in the surface heat fluxes. In a second configuration of the model with four ensemble members and 1.0 Sv of freshwater forcing, both the topography and surface heat flux corrections were prescribed. A final set of four ensemble members was performed with 0.1 Sv freshwater forcing with both topography and surface heat flux corrections prescribed (see Atwood et al. 2020, for more details).

2.1.5 Volcanic forcing

The climate response to volcanic forcing is analyzed separately for volcanic events localized in the NH extratropics, SH extratropics and tropics. Volcanic events from two different types of simulations are analyzed: (1) volcanic forcing only experiments and (2) last millennium simulations with all climate forcings.

The volcanic forcing only simulations consist of 5 CESM Last Millennium Ensemble (LME) volcanically simulations (with separate composites constructed from each simulation for volcanic eruptions located in the NH, SH and tropics—making 15 CESM composites) and an ensemble of simulations with the Norwegian Earth System Model Version 1M (NorESM) mimicking a highlatitude Northern Hemisphere (NH) summer eruption (the Laki eruption in Iceland; Pausata et al. 2015a, b). In the NorESM simulations, 100 Tg of SO₂ and dust was added to the upper atmosphere over a four month period starting on June 1st to simulate the Laki eruption. Eruptions were prescribed at a different starting year of a transient historical simulation (1850–2005) for each of the 48 ensemble members. 3 composites each consisting of 16 ensemble members are formed to be consistent with the number of eruptions in the last millennium composites (discussed below). ΔP forced by the volcanic eruptions in NorESM is diagnosed from the composite response in the year after the volcanic event. The NorESM volcanic forcing runs are compared against control runs in the same model

that were branched from the same transient historical simulation but with no prescribed volcanic forcing.

The response to volcanic forcing is also assessed from selected PMIP3 all-forcing last millennium (LM) transient simulations (CCSM4 and GISS Model E Ensemble Members 122, 125, and 128). In the last millennium simulations, ΔP forced by volcanic eruptions is diagnosed from the composite response in the years after a volcanic event minus that in the closest 5 years preceding the event with minimal volcanic activity. Specifically, for each eruption, the monthly precipitation response was calculated from months with AOD > 0.02 up to 2 years before and after the peak of the eruption and compared to the control climatology, which was taken to be the climatology of the closest 5-year period prior to the onset of the event with minimal volcanic activity (defined as global mean AOD summed over the 5 year period < 0.01). Tropical volcanic events are defined as volcanic events with peak globally-averaged AOD > 0.1 and an AOD difference between the hemispheres of less than 25%. Extratropical volcanic events are similarly defined but with a hemispherically-averaged AOD at least 25% greater in one hemisphere. This procedure results in composites for each simulation that consist of 9–20 events in each region (NH, SH, and tropics—see Atwood et al. 2020, for more details).

2.2 Methodology for defining optimal precipitation shifts, intensifications, and contractions

We characterize the forced ΔP in terms of shifts, intensifications and contractions of the unforced (control) climatological tropical precipitation by optimally geometric manipulating the control precipitation to best match the forced precipitation. We begin by evaluating the optimal shift acting in isolation. To search for the optimal shift, the unperturbed (pre-industrial) zonal mean precipitation, $P_{PI}(\theta)$, is shifted in latitude, θ , both northward and southward by S degrees latitude in increments of 0.02° up to 5°. Mathematically:

$$P_{SHIFT}(\theta) = P_{PI}(\theta - S). \quad (1)$$

For each value of S in the search algorithm, the fraction of ΔP explained by a shift of S ($FRAC_{SHIFT}$) is defined as:

$$FRAC_{SHIFT} = 1 - \frac{\sqrt{\langle (P_{FORCED} - P_{SHIFT})^2 \rangle}}{\sqrt{\langle \Delta P^2 \rangle}} \quad (2)$$

where angled brackets, $\langle \rangle$, denote spatial averages over the tropics (defined as equatorward of 20°). The fraction of ΔP explained by the shift is negatively proportional to the root mean square (RMS) difference between the shifted precipitation (P_{SHIFT}) and the target precipitation (P_{FORCED})

normalized by the root mean square of ΔP . If P_{SHIFT} perfectly matches P_{FORCED} , the RMS difference is zero and the fraction explained is 1. Whereas for a shift of zero, $P_{FORCED} - P_{SHIFT,0} = \Delta P$ so the numerator and denominator are equal and the $FRAC_{SHIFT} = 0$. The optimal shift is chosen such that $FRAC_{SHIFT}$ is maximized or, equivalently, the RMS error between the shifted precipitation and the target precipitation (P_{FORCED}) is minimized.

To demonstrate the optimization algorithm, consider the precipitation response to freshwater forcing in the CCSM4 model shown by the green line in Fig. 1B which has enhanced tropical precipitation in the SH tropics relative to that in the unforced simulation (P_{PI} , black line). The goal is to meridionally translate the pre-industrial precipitation (P_{PI} , black line) to optimally fit P_{FORCED} (green line). The optimal shift is determined to be -1.7° (with negative indicating southward) and the optimally shifted precipitation is shown by the blue curve. $FRAC_{SHIFT} = 0.25$ which indicates that 25% of ΔP is explained by the shift. By construction, the optimally shifted precipitation has the same shape as P_{PI} but is meridionally translated; the significant mismatch between P_{SHIFT} and P_{FORCED} is associated with changes in the amplitudes of the peaks. The optimally shifted precipitation matches P_{FORCED} significantly better than P_{PI} but it is far from a perfect match. We note the optimal shift is evaluated to within 0.02° latitude which is a finer resolution than the model output. These sub-grid scale shifts impact precipitation changes on the coarser model grid.

Next we optimally shift and intensify P_{PI} in conjunction to best match P_{FORCED} to ask: what additional fraction of ΔP can be explained by introducing an optimal intensification of the climatological precipitation (relative to the optimal shift only)? Mathematically, the combined shift and intensification of P_{PI} is

$$P_{SHIFT,INT}(\theta) = I \cdot P_{PI}(\theta - S), \quad (3)$$

where I is the (dimensionless) intensification scalar. We calculate $P_{SHIFT,INT}$ for values of I between 0.8 and 1.2 in increments of 0.01 and over the S values previously considered in the shift only case. The optimal values of S and I are defined as those for which the RMS difference between $P_{SHIFT,INT}$ and P_{FORCED} is minimized—noting that the optimal value of S for the combined shift and intensification need not equal that for the optimal shift only. The additional fraction of ΔP explained by the intensification, $FRAC_{INT}$, is defined as the improvement of RMS error in the fit to P_{FORCED} relative to that of the optimally shifted only precipitation, normalized by RMS ΔP :

$$FRAC_{INT} = \frac{\sqrt{\langle (P_{FORCED} - P_{SHIFT})^2 \rangle}}{\sqrt{\langle \Delta P^2 \rangle}} - \frac{\sqrt{\langle (P_{FORCED} - P_{SHIFT,INT})^2 \rangle}}{\sqrt{\langle \Delta P^2 \rangle}}. \quad (4)$$

A clear example of the how the intensification mode contributes to explaining ΔP is demonstrated by the optimal fit to the simulated precipitation response to $4XCO_2$ in the FGOALS model (Fig. 1A). In this case, the shift alone (optimal value of 0.5° northward) describes a very small fraction of ΔP (2%) whereas the combined shift and intensification (optimized $I = 1.16$ intensification) explain 39% of ΔP . The difference in fraction of ΔP explained between these two optimized fits (37%) is defined as $FRAC_{INT}$.

Next, we introduce a meridional contraction of P_{PI} in conjunction with the shifting and intensifying modes using the form

$$P_{SHIFT,INT,CON}(\theta) = I \cdot P_{PI}\left(\frac{1}{C} \cdot (\theta - S)\right), \quad (5)$$

where C is the contraction scalar with $C > 1$ corresponding to an expansion and $C < 1$ corresponding to a contraction. We search over values of C between 0.8 and 1.2 in increments of 0.01 and over the S and I values previously considered. The optimal values of S , I and, C are defined as those for which the RMS difference between $P_{SHIFT,INT,CON}$ and P_{FORCED} is minimized—noting that the optimal value of S and I for the optimal $P_{SHIFT,INT,CON}$ need not equal those defined for $P_{SHIFT,INT}$ and/or P_{SHIFT} . The additional fraction of ΔP explained by the contraction, $FRAC_{CON}$, is defined as the improvement of RMS error in the fit to P_{FORCED} relative to that of the optimally shifted and intensified precipitation ($P_{SHIFT,INT}$) normalized by the RMS ΔP :

$$FRAC_{CON} = \frac{\sqrt{\langle (P_{FORCED} - P_{SHIFT,INT})^2 \rangle}}{\sqrt{\langle \Delta P^2 \rangle}} - \frac{\sqrt{\langle (P_{FORCED} - P_{SHIFT,INT,CON})^2 \rangle}}{\sqrt{\langle \Delta P^2 \rangle}}. \quad (6)$$

The improved fraction of ΔP explained due to introducing an optimal contraction can be visualized in Fig. 1A by the mismatch between P_{FORCED} (green) and $P_{SHIFT,INT,CON}$ (orange) as compared to that of $P_{SHIFT,INT}$ (red). In the example of the simulated precipitation response to $4XCO_2$ in the FGOALS model (Fig. 1A), the intensity of the bimodal peaks (near 7° N and 7° S) in the optimized $P_{SHIFT,INT}$ (before the contraction mode is introduced) is too small

whereas the intensity of the precipitation on the poleward flanks of the peaks is too large and, thus, further increasing the I scalar in $P_{SHIFT,INT}$ to match the peaks height increases the RMS mismatch with P_{FORCED} . However, introducing a contraction in conjunction with a shift and intensification of the precipitation distribution allows the optimal solution to match both the increased precipitation in the peaks of the distribution and the nearly unchanged precipitation on the flanks. The combination of all three optimized modes ($P_{SHIFT,INT,CON}$) explains an impressive 75% of ΔP . This improved fit relative to $P_{SHIFT,INT}$, which only explains 39% of ΔP , is attributed to the contraction mode ($FRAC_{CON} = 36\% = 75 - 39\%$).

We have chosen to apply the precipitation modes in the order: (1) shift, (2) intensification, (3) contraction. This methodology answers the following sequence of questions: (1) What fraction of ΔP is described by an optimal shift alone? (2) How much additional ΔP can be described by adding an optimal intensification in conjunction with the shift? and (3) How much additional ΔP can be described by introducing an optimal contraction in addition to the shift and intensification? Because the three precipitation modes are not generally spatially orthogonal, the order of applying the modes does impact the resultant $FRAC_{SHIFT}$, $FRAC_{INT}$ and $FRAC_{CON}$. In practice, the shifting mode is nearly spatially orthogonal to the other modes whereas the contraction and intensification are not. This characteristic can be understood as follows; since precipitation is larger in the deep tropics (i.e. near the equator) than at the edges of the tropical domain, an expansion of P_{PI} ($C > 1$) results in a domain wide intensification and, thus, projects onto the intensifying mode. Qualitatively similar results for $FRAC_{SHIFT}$, $FRAC_{INT}$ and $FRAC_{CON}$ are found for the five alternative permutations of the order of modes aside from one exception: the value of C found for optimizing ΔP is significantly impacted by whether contraction is introduced before or after the intensification mode due to the previously mentioned increase in tropical domain average precipitation that results from meridional expansion alone. For this reason, we report the modal parameters (S , I and, C) that result from optimizing all three modes simultaneously. We report $FRAC_{SHIFT}$, $FRAC_{INT}$ and, $FRAC_{CON}$ that result from the specific order of modes outlined above.

3 Results

We begin by characterizing the ensemble mean and spread of ΔP under each forcing scenario in terms of optimal shifts, intensifications and contractions of unperturbed precipitation (P_{PI}). In Sect. 3.2, we then generalize across experiment type to assess the relative importance of shifts, intensifications and contraction for describing tropical precipitation

changes. In Sect. 3.3, we compare the magnitude of optimal shifts (S) to other common metrics of ITCZ shifts diagnosed from the same simulations and discuss the differences.

3.1 Characterization of tropical precipitation changes in response to different forcings

3.1.1 Last glacial maximum and 4XCO₂

The tropical precipitation changes from the cold LGM climate (solid blue line in Fig. 2A) to the pre-industrial (black line) and from the pre-industrial to the warm 4XCO₂ climate (solid red line) are best characterized as an intensification and meridional contraction of the precipitation distribution as the planet warms. The precipitation contraction with warming is visually evident from the equatorward migration of the bi-modal precipitation peaks in warmer climates, especially the SH peak under 4XCO₂ forcing. The optimally shifted, intensified and contracted fit ($P_{SHIFT,INT,CON}$) to P_{FORCED} is shown by the dashed lines in Fig. 2A, which captures a large fraction of ΔP ; $P_{SHIFT,INT,CON}$ explains 62% and 61% of the ensemble mean ΔP for the LGM and 4XCO₂ simulations, respectively. The optimal modal fit of the LGM precipitation ($P_{SHIFT,INT,CON}$) features a robust decrease in the intensity of tropical precipitation across models ($I = 0.91 \pm 0.02$) and an expansion of the precipitation distribution ($C = 1.04 \pm 0.02$) where the stated range is two standard deviations of the ensemble mean, roughly corresponding to the 95% confidence interval (values are shown in the table inset of Fig. 2A). In contrast, in response to 4XCO₂ forcing there is robust intensification of tropical precipitation ($I = 1.13 \pm 0.02$) and a contraction in the precipitation distribution ($C = 0.89 \pm 0.02$). There is also a modest but robust southward shift in precipitation under LGM forcing ($S = -0.4^\circ \pm 0.2^\circ$), whereas the shift under 4XCO₂ is not robust—a southward shift is found in 9 models and northward shift is found in 13 models, in agreement with the analysis of Donohoe and Voigt (2015).

The optimal shift under LGM forcing is southward in 11 of the 13 simulations (abscissa in Fig. 3A) with an ensemble mean value of -0.4° and is $< 1^\circ$ in the majority of models. The magnitude of these shifts is almost an order of magnitude less than those inferred at regional scales from paleoclimate reconstructions such as the 7° southward shift of the Atlantic ITCZ suggested by Arbuszewski et al. (2013). Similarly, the magnitude of the optimal shift in response to 4XCO₂ is less than 1° in all ensemble members (red dots in Fig. 3A). In addition to the small magnitude of the optimal shift, the shifting mode explains a small fraction of ΔP under both LGM and 4XCO₂ forcing; the ensemble average $FRAC_{SHIFT}$ is 4% and 2% for the LGM and 4XCO₂ simulations and

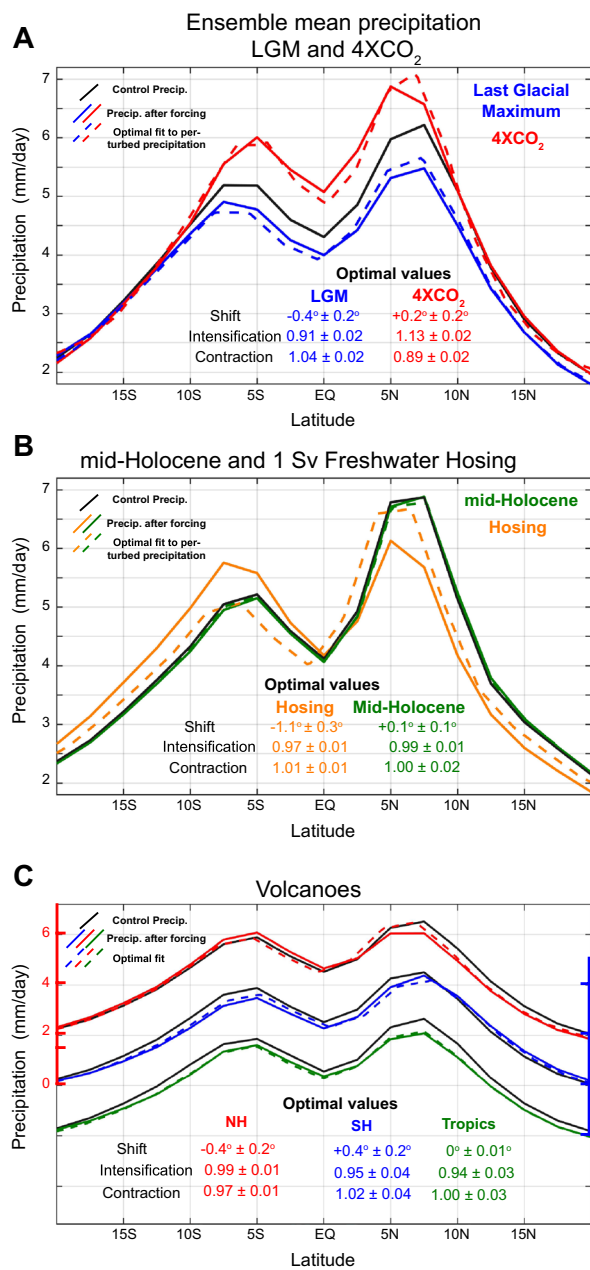


Fig. 2 Ensemble mean, zonal mean and annual mean precipitation for pre-industrial simulations (solid black) and forced simulations (solid colors) with the optimal fit to the forced precipitation shown in dashed colors for the: **A** Last Glacial Maximum (blue) and 4XCO₂ (red) simulations; **B** Mid-Holocene (green) and 1 Sv North Atlantic Freshwater Hosing (orange) and **C** volcanic forcing simulations subdivided into eruptions originating in the Northern Hemisphere (red), Southern Hemisphere (blue) and tropics (green). Results from each volcanic forcing region have been offset on the ordinate by 2 mm per day (with the PI distribution repeated) for visual purposes as indicated by the colored ordinate axes. Ensemble mean optimal parameters and their inter-model spread (defined as 2 standard deviations of the mean) are shown in the inset tables

exceeds 10% in only two of the LGM simulations and one of the 4XCO₂ simulations (Fig. 4A).

In addition to the robust ensemble mean intensification and contraction of tropical precipitation under global warming, the intensification and contraction are highly (negatively) correlated across model simulations, with correlation coefficients of -0.95 and -0.52 for the LGM and 4XCO₂ simulations, respectively (Fig. 3B). This result suggests that the degree of contraction and the degree of intensification of the tropical precipitation distribution in response to forcing go hand in hand. We return to this point in Sect. 3.2. The intensification and contraction modes each explain a significantly greater fraction of ΔP than the shift mode in response to LGM and 4XCO₂ forcings (Fig. 4A). The intensification mode explains 48% and 30% of ΔP in the LGM and 4XCO₂ simulations, respectively, with values exceeding 10% in all of the LGM simulations and 19 of 22 of the 4XCO₂ simulations (Fig. 4A). The contraction mode explains 10% and 29% of ΔP in the LGM and 4XCO₂ simulations, respectively, with values exceeding 10% in 7 of 13 of the LGM simulations and 20 of 22 of the 4XCO₂ simulations (Fig. 4A). These results collectively demonstrate that contractions and intensifications of tropical precipitation respond robustly to CO₂ and LGM forcing and better characterize the changes in tropical precipitation changes than does meridional shift.

3.1.2 Freshwater hosing

The ensemble mean tropical precipitation under 1 Sv of freshwater hosing of the North Atlantic (solid orange in Fig. 2B) features a reduction of the precipitation maximum in the NH and an amplification of the precipitation maximum in the SH relative to precipitation in the PI simulation (black solid line). ΔP in response to freshwater hosing is best characterized by the shifting mode (ensemble mean $\text{FRAC}_{\text{SHIFT}}$ of 20%—Fig. 4A) with a robust ensemble mean southward shift of $-1.1^{\circ} \pm 0.3^{\circ}$ (Fig. 2B). ΔP in response to 0.1 Sv of freshwater forcing (4 CCSM4 simulations—not shown) is much smaller in magnitude than the response to 1 Sv of freshwater forcing with a similar spatial characterization with an amplification of the SH precipitation peak and reduction of the NH peak. The ensemble mean ΔP response to 0.1 Sv is not significantly different than 10% of the ensemble mean ΔP in response to 1 Sv of hosing in the CCSM4 (12 simulations) with an ensemble mean (southward) optimal shift (S) of $-0.12 \pm 0.03^{\circ}$ in response to 0.1 Sv as compared to $-1.1^{\circ} \pm 0.3^{\circ}$ in response to 1 Sv. This result indicates that given the number of simulations considered, we can not reject the null hypothesis that the ΔP response to hosing is linear with respect to the magnitude of the prescribed freshwater flux.

In the 1 Sv freshwater hosing simulations, there is also a modest but robust reduction of the ensemble mean

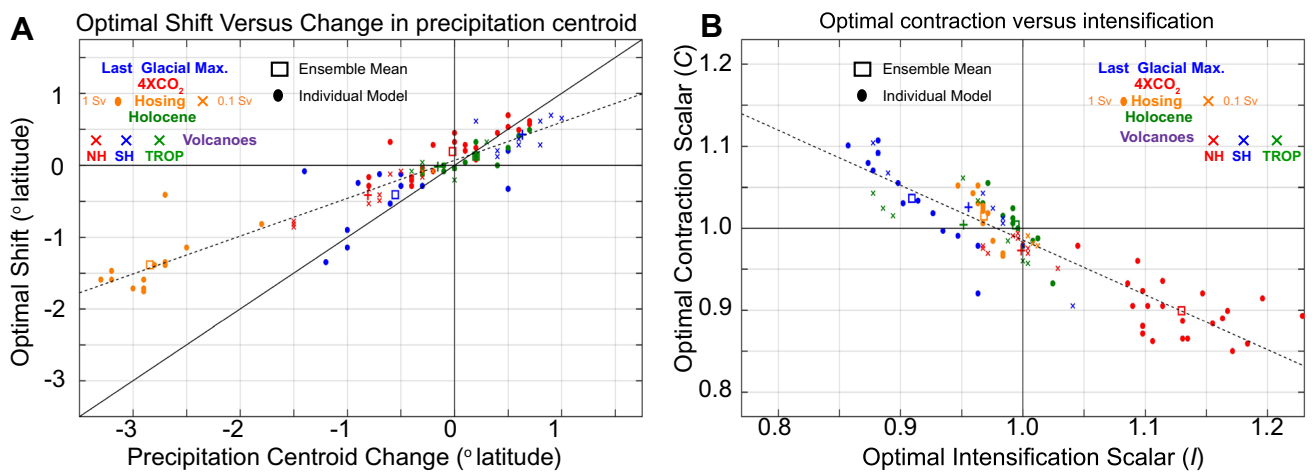


Fig. 3 Optimal shift, contraction and intensification parameters for the zonal and annual mean precipitation changes in response to LGM (blue dots), 4XCO₂ (red dots), Mid-Holocene (green dots), freshwater hosing (orange dots for 1 Sv and crosses for 0.1 Sv) and volcanic forcing which are further subdivided into volcanoes in the Northern Hemisphere (NH—red crosses), Southern Hemisphere (SH—blue crosses) and, Tropics (TROP—green crosses). **A** Optimal shift (ordinate) versus the change in precipitation centroid (abscissa) that is

commonly used to quantify ITCZ shifts. The 1:1 line is shown by the solid black line and the linear best fit is shown by the dashed black line. **B** Optimal contraction scalar (ordinate) versus optimal intensification scalar (abscissa). Dots (and smaller crosses for volcanoes) represent individual models and the open squares (larger plus signs for volcanoes) show the ensemble mean of simulations for each forcing experiment. The ensemble mean square for the hosing simulations is the mean of the 1 Sv freshwater forcing simulations only

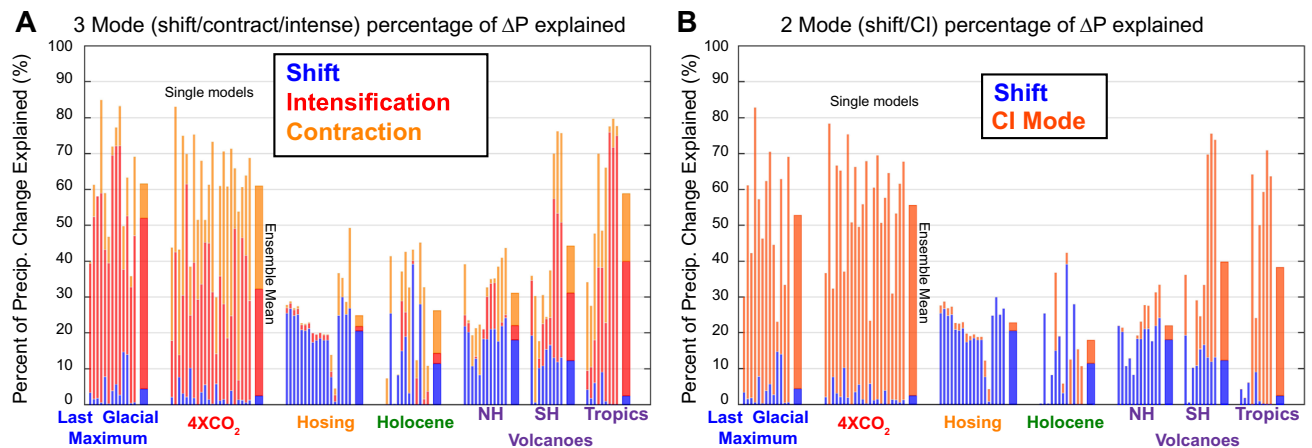


Fig. 4 The percentage of ΔP explained by each mode of tropical precipitation changes in the ensemble of forced simulations. Results are grouped by forcing type with individual models shown by thin bars and the ensemble average shown in the thick bar to the right. **A** Three mode optimization with percentages defined starting from the shifting mode only (blue) then adding the intensification mode (red) and the

adding the contraction (orange). **B** Two mode optimization with percentages defined starting from the shifting mode (blue) then adding the combined contraction-intensification mode (CI—reddish orange) with the ratio of the contraction to intensification defined from the linear best fit across all simulations shown in Fig. 1B

precipitation ($I = 0.97 \pm 0.01$) that explains a small fraction of ΔP (1%), whereas the ensemble mean contraction is not significantly different from zero. Despite the ambiguity of the direction of contraction across ensemble members (Fig. 3B), the contracting mode describes a non-negligible fraction of ΔP (4%) across the ensemble members and up to 22% in individual ensemble members (Fig. 4A). We note that, even though the shifting mode explains a larger fraction ΔP than the other two modes, overall the ΔP is poorly

characterized (26%) by the geometry of the optimal modes considered here, as is evident in the mismatch between the optimal fit and P_{FORCED} (c.f. the solid and dashed orange lines in Fig. 2B). The reason for this mismatch is as follows: the three modes chosen in this study do not allow for the relative magnitudes of the precipitation peaks in the NH and SH to change but, rather, only allow the peaks to simultaneously increase/decrease (via the intensity mode), translate together (via the shift mode) or move closer/farther apart

(via the contraction mode). If we were, instead, to employ a precipitation mode that optimized the intensity of the precipitation differentially in the NH and SH, the optimized fit would better match P_{FORCED} under freshwater forcing. We return to this point in Sect. 3.3.

3.1.3 Mid-Holocene

The ensemble average ΔP in response to mid-Holocene forcing is small in magnitude compared to that of other forcings considered here (green line in Fig. 2B). Furthermore, there is no robust direction of the optimal shift, intensification, and contraction across the ensemble of experiments. For individual ensemble members, the magnitude of simulated ΔP in response to mid-Holocene forcing is significantly smaller (approximately 20% of) that in the other forcings considered here with an ensemble average tropical domain RMS of ΔP equal to 0.08 mm/day as compared to 0.37, 0.40 and 0.34 mm/day in the LGM, 4XCO₂ and hosing simulations, respectively. Additionally, Fig. 4A shows that the total fraction of ΔP explained by all three optimal modes is significantly smaller for the mid-Holocene simulations (ensemble average of 25%) than for the LGM and 4xCO₂ simulations (ensemble averages of 61% and 61%, respectively). The contraction mode describes the largest fraction of ΔP across the mid-Holocene ensemble (12%) followed by the shifting mode (11%) whereas the intensification mode is relatively inefficient at characterizing ΔP (2%). We note that there are robust seasonally and longitudinally inhomogeneous changes in simulated tropical precipitation under mid-Holocene forcing (Braconnot et al. 2007b; Liu et al. 2018) but the imprint of these changes on the zonal and annual mean ΔP is small and poorly characterized by the modes of tropical precipitation considered here.

3.1.4 Volcanic forcing

The tropical precipitation response to volcanic forcing is separated into ensemble averages of NH volcanoes (red line—Fig. 2C), SH volcanoes (blue line) and, tropical volcanoes (green line). The ordinate scale for each ensemble average (NH, SH, and tropical) are offset for visual purposes. The ensemble mean P_{FORCED} in response to NH volcanic events features a reduction in the amplitude of the NH precipitation peak and an enhancement of the SH precipitation peak relative to P_{PI} . This precipitation response is qualitatively similar to that seen under North Atlantic freshwater hosing but with reduced magnitude. The response to SH volcanoes is nearly a mirror image of the response to NH volcanoes but with an additional tropical domain average precipitation reduction such that a reduction in the amplitude of the SH precipitation peak is the primary feature of ΔP . ΔP under extratropical volcanic forcing is robustly characterized

by an ensemble mean shift away from the source of volcanic forcing: the optimal shift in response to NH volcanic forcing is southward in all 15 ensemble members (ensemble mean $-0.4^\circ \pm 0.2^\circ$) and the optimal shift in response to SH volcanic forcing is northward in all nine ensemble members (ensemble mean $0.4^\circ \pm 0.2^\circ$). In addition to the shift under extratropical volcanic forcing, there is also a robust de-intensification of precipitation under SH volcanic forcing and a contraction of precipitation under NH forcing. These two robust ensemble mean responses (de-intensification under SH forcing, contraction under NH forcing) are most pronounced in the three GISS Model E members, which have a larger magnitude volcanic forcing than the other simulations (see Atwood et al. 2020, for a discussion) whereas the shifting response to extratropical volcanoes is robust across models (Fig. 4A).

Although the intensifying and contracting modes explain a small fraction of the ensemble mean ΔP in response to extratropical volcanic forcing, these modes do explain a significant fraction of ΔP within individual models. The intensifying and contracting modes explain 19% (4%) and 10% (13%) of ΔP across the SH (NH) volcanic forcing ensembles (Fig. 4A) as compared to 12% (18%) for the shifting mode. This result suggests that, while the tropical precipitation is clearly redistributed away from the cooled hemisphere in response to extratropical volcanic forcing, the precipitation response to extratropical volcanic forcing is poorly characterized by a meridional translation of the climatological precipitation. As was discussed for ΔP under freshwater hosing, the shifting mode cannot capture the opposing changes in the magnitude of the NH and SH precipitation peaks and, thus, fails to capture a large fraction of ΔP .

In response to tropical volcanoes, the ensemble mean P_{FORCED} features a nearly latitudinally homogeneous reduction in precipitation throughout the tropical domain with no discernible change in the shape of the distribution (green line in Fig. 2C). The optimal characterization of the ensemble mean ΔP under tropical volcanic forcing is a robust reduction in intensity ($I = 0.94 \pm 0.03$) with no statistically significant contraction or shift. Across the ensemble members, the intensification mode explains 38% of ΔP whereas the contraction explains 19% despite the differing direction of contraction/expansion across the ensemble members (contracting in 5 of 9 members and expanding in 4 of 9 members). The shifting mode explains very little (2%) of ΔP in response to tropical forcing which suggests that, in the particular case of tropical volcanic forcing, changes in energy input to the tropical atmosphere (Schneider et al. 2014) has minimal impact on the ITCZ location. We speculate that the insensitivity of ITCZ shifts to tropical energy input in this model is a consequence of a mean state (annual mean) ITCZ which is near the equator and, thus, there is

minimal area between the energy flux equator and geographic equator.

Our general finding that the tropical precipitation is redistributed away from extratropical volcanoes and is reduced in response to tropical volcanoes agrees with the conclusions of Colose et al. (2016). Previous work has demonstrated that the precipitation response to volcanic forcing is “El Nino-like” for eruptions in the NH (Stevenson et al. 2016) and it is possible that the methodology for defining the precipitation response to volcanic forcing used here includes a portion of the transient El Nino response. However, the tropical precipitation response to El Nino in observations is primarily characterized by a contraction of precipitation with a very modest shift (not shown) and, thus, it is unlikely that the transient ENSO response to volcanic forcing substantially impacts the diagnostics (or explanatory power) of the shift mode.

3.2 The emergence of a joint contracting and intensifying mode of tropical precipitation

In response to each of the forcings, the optimal contraction (C) and intensification (I) scalars are remarkably anti-correlated ($R = -0.91$, Fig. 3B) with a least squares regression slope of $\frac{C}{I} = -0.8$ (the dashed black line in Fig. 3B). The direction of the response in C and I is remarkably consistent across models in response to the same forcing. In particular, tropical precipitation expands and de-intensifies under LGM forcing (blue dots in Fig. 3B are in the $C > 1$ and $I < 1$ quadrant) and expands and intensifies under $4XCO_2$ (red dots in Fig. 3B are in the $C < 1$ and $I > 1$ quadrant). These results suggest that tropical precipitation contractions and intensifications are tightly coupled and the direction of these forced changes are consistent across models, though the magnitude (of the combined contraction/intensification) is model dependent. Moreover, the scaling between the contraction (C) and intensification (I) scalars seems relatively consistent across models and climate forcings.

3.2.1 Physical basis of the contracting and intensifying mode of tropical precipitation

We first evaluate if the relationship between C and I is a consequence of conservation of tropical domain average precipitation. Given that C and I both change the tropical domain average precipitation (which increases with both increasing I and decreasing C), one would expect an anticorrelation between C and I if the tropical domain average precipitation was nearly unchanged. We demonstrate that the linear relationship between C and I seen in Fig. 3B ($\frac{C}{I} = -0.8$) is significantly different than that expected from conservation of tropical precipitation through the following exercise: (1) P_{PI} in each model is contracted/expanded (via random values of C in

equation 5), (2) we find the value of I for each C that restores the tropical domain average of the contracted/expanded precipitation to that of P_{PI} . The resultant tropical domain average conserving relationship between C and I is $\frac{C}{I} = -2.0$ which differs from that seen across the climate forcing simulations. Therefore, the tight correlation between C and I has a physical basis and is not merely a consequence of conservation of domain average precipitation.

We next evaluate the hypothesis that the tight relationship between C and I under climate change is a result of thermodynamic considerations. Following Held and Soden (2006), if atmospheric circulation and relative humidity are climate state invariant, then the change in precipitation minus evaporation, $\Delta(P-E)$, is given by:

$$\Delta(P-E) = (P-E)\alpha\Delta T \quad (7)$$

where α is the linearized dependence of saturation vapor pressure on temperature in the Clausius Clapeyron equation and ΔT is the local temperature change. Hence, provided that the ΔT has a weaker spatial structure in the tropics than the climatological $(P-E)$, thermodynamic constraints suggest that the spatial structure of $(P-E)$ is climate state invariant but intensifies with warming and de-intensifies with cooling. Thus, thermodynamic constraints are equivalent to $\Delta(P-E)$ being explained entirely by a geometric mode akin to the intensification mode but acting on the climatological spatial distribution of $(P-E)$.

The thermodynamic prediction for $(P-E)$ under $4XCO_2$ with scaling chosen to match the ensemble mean global integral of the absolute value of $(P-E)$ is shown by the orange lines in Fig. 5. Under $4XCO_2$, the change in E is nearly spatially homogeneous over the tropical domain (c.f. the solid red and dashed red line in Fig. 5A) and, thus, $\Delta(P-E)$ mimics the spatial structure of ΔP . Importantly, the shape of $\Delta(P-E)$ differs significantly from the climatological $(P-E)$ and, thus, the change in $(P-E)$ predicted from thermodynamic constraints (orange line in Fig. 5B) is a poor match to that realized in model simulations (black lines in Fig. 5B). Specifically, the latitude of zero $(P-E)$ robustly contracts toward the equator under $4XCO_2$ and the bi-modal peaks in $(P-E)$ also shift equatorward. Thermodynamic constraints explain only 25% of the ensemble mean $\Delta(P-E)$ under $4XCO_2$ and 34% in the LGM simulations (not shown); similar percentages are found in individual models. This is roughly half of the fraction of the ΔP that is explained by a combined mode of contraction and intensification (53% for $4XCO_2$ and 48% for the LGM) described in Sect. 3.3. From this we conclude that the tight relationship between contractions and intensifications are neither a consequence of conservation of tropical domain average precipitation nor thermodynamic considerations and, rather, likely result from robust changes in atmospheric dynamics under global warming and cooling.

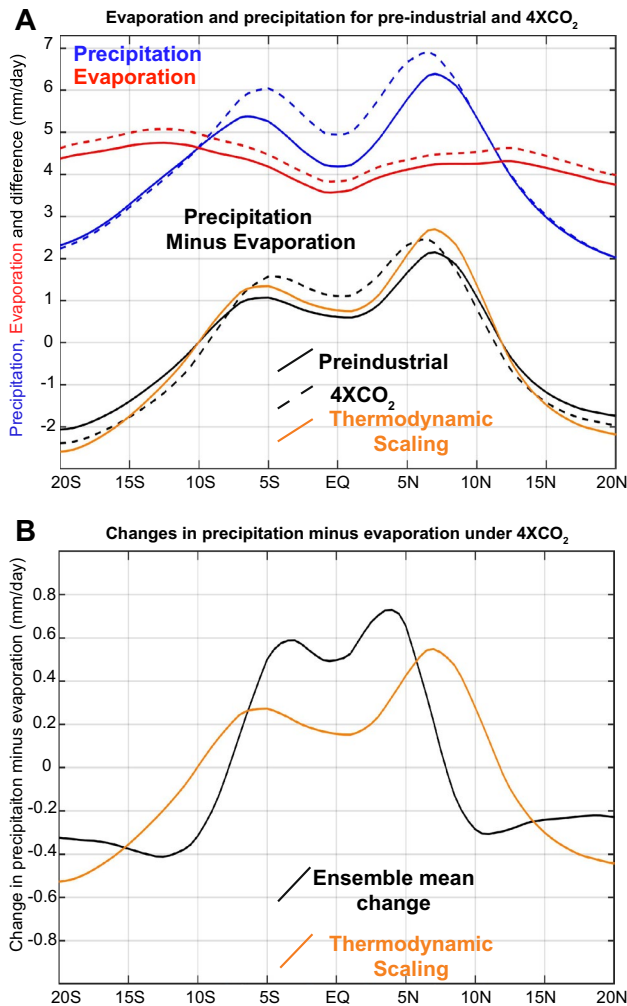


Fig. 5 **A** Ensemble mean, zonal mean and annual mean precipitation (blue), evaporation (red) and precipitation minus evaporation (black) for the pre-industrial simulations (solid lines) and 4XCO₂ simulations (dashed lines). The thermodynamic scaling of Held and Soden (2006) which predicts precipitation minus evaporation will scale with water vapor content of the atmosphere is shown in the orange line. **B** The ensemble mean change precipitation minus evaporation (black) compared to the thermodynamic prediction

3.2.2 Explanatory power of the joint contracting and intensifying mode of tropical precipitation

Given C and I are highly (anti-) correlated across the ensemble of climate forcing simulations, we now define a combined mode of contraction and intensification constrained by the linear best fit relationship of $\frac{C}{I} = -0.8$. In other words, we require that C and I used to define the optimal fit to P_{FORCED} in Eq. (5) follow $= -0.8 I$, thus, reducing the number of free parameters used to optimize the fit to P_{FORCED} . We refer to this combined mode of contraction/intensification or expansion/deintensification as the CI mode. We repeat our optimal characterization ΔP using two

modes—the shift and CI mode—as opposed to the three original independent modes (shift, contraction and, intensification). Since we are fitting for two free parameters instead of three free parameters using the same geometric basis, a smaller fraction of ΔP will be described by the two mode methodology as compared to the three mode methodology. However, the advantage of this approach is it simplifies the characterization of tropical precipitation changes and reduces the likelihood of statistical artifacts.

The fraction of ΔP explained by the two mode characterization across all forcing scenarios is shown in Fig. 4B alongside that of the three mode characterization in Fig. 4A. We note, that since the shift mode is optimized to best fit P_{FORCED} before optimizing the other modes in the calculation, $FRAC_{SHIFT}$ is unchanged between the three mode and two mode characterizations. In the LGM and 4XCO₂ simulations, the CI mode explains a very large fraction (48% and 53%, respectively) of ΔP , respectively. There is a modest reduction (9% in the LGM simulations and on 5% in the 4XCO₂ simulations) in ΔP explained due to switching from a three parameter characterization to the two parameter characterization (c.f. panel 4A, B) suggesting that the CI mode efficiently represents ΔP across these simulations (and across the different models) with little loss of explanatory power. Additionally, the precipitation response to tropical volcanoes, and to some extent SH volcanoes, is well characterized by the CI mode (explaining 36% and 28% of ΔP respectively). In contrast, in response to freshwater hosing and NH volcanoes, the CI mode explains very little of ΔP , as is expected given that ΔP for these simulations is dominated by the shift mode. Under mid-Holocene forcing, combining the contraction and intensification modes into a single CI mode results in reduction of ΔP explained by 8%, from 26% in the three mode characterization to 18% for the two mode characterization. Similarly, under volcanic forcing the fraction of ΔP explained by the two mode optimization (32%) is reduced by 11% relative to that of the three mode optimization (43%). These significant fractional loss of explanatory power by the two mode optimization results from the optimal contraction and intensification scalars in individual ensemble members diverging from the ensemble mean best fit line (Fig. 3B).

Overall, the CI mode is an efficient representation of ΔP in the simulations characterized by global warming and cooling (e.g. LGM and 4XCO₂) and only modestly reduces the explanatory power of geometric modes for describing ΔP under mid-Holocene, freshwater hosing and volcanic forcing.

3.3 Magnitude and explanatory power of the shifting mode

The optimal shift (S) defined in this study provides a metric to quantify an ITCZ shift in terms of its most literal

definition, that is, a meridional translation of the climatological precipitation pattern. This metric can be compared to other commonly used metrics of “ITCZ shifts” such as changes in the precipitation centroid— P_{CENT} , defined as the latitude that demarcates regions of equal area weighted precipitation between 20° S and 20° N (Frierson and Hwang 2012)—or changes in the precipitation weighted latitude (“moments”) of the tropical precipitation distribution (Adam et al. 2016a). We present the relationship between S and the change in P_{CENT} in Fig. 3A due to the prominence of the latter metric in the paleoclimate (McGee et al. 2014) and dynamics (Donohoe et al. 2013) literature. S and the change in P_{CENT} are very well correlated ($R = 0.93$) across the ensemble of different forcings but the magnitude of S is approximately half of the P_{CENT} change (the slope of the linear best fit in Fig. 3A is 0.52) indicating that the P_{CENT} metric of “ITCZ shifts” is more sensitive to the patterns of ΔP realized in model simulations than the optimal shift metric S . Changes in S are generally small in magnitude (ordinate of Fig. 3B): S is less than 1° in all 4XCO₂, mid-Holocene and volcanic forcing simulations and only exceeds 1° in magnitude for two of the 13 LGM simulations. The largest magnitude S values are found in response to freshwater hosing with magnitudes exceeding 1° in 15 of 18 simulations. S is less than 2° in magnitude across all simulations.

It is tempting to conclude from the results above that the optimal shift (S) is a less sensitive metric for measuring shifts tropical precipitation than P_{CENT} . We demonstrate below that this is the wrong interpretation and, in fact, for the case of a ΔP that is well characterized by a meridional translation of P_{PI} , S is a *more sensitive* metric of ITCZ shifts than P_{CENT} . To see this point, we first analyze the quantitative relationship between P_{CENT} and the optimal shift S for the case of a ΔP that is perfectly described by a meridional translation of the climatological precipitation in the following set of analysis: (1) the pre-industrial precipitation (P_{PI}) is meridionally translated via Eq. (1) north and south in increments of 0.1° up to 5° N/S, (2) for each prescribed S , we calculate the resulting change in P_{CENT} relative to that calculated from P_{PI} . We find that the change in P_{CENT} is approximately one half of prescribed S for all cases (regression coefficient = 0.51). This suggest that S is a more sensitive metric for meridional translations of the ITCZ than the P_{CENT} change metric which can be understood as follows. For the case of a prescribed 5° northward translation of P_{PI} , the precipitation that was originally between 15° and 20° N has shifted out of the tropical domain defined by P_{CENT} whereas the precipitation originally between 25° and 20° S has entered the tropical domain. P_{CENT} shifts less than the prescribed 5° northward translation because, using the gravitational analogy, it now feels the gravitational pull of the precipitation that has entered the tropical domain from the southern edge (and has lost the gravitational pull

of the precipitation that has exited the tropical domain to the North). P_{CENT} can only change as much as S if the precipitation is zero at the edge of the tropical domain. More generally, for the case of a pure translation of the climatological precipitation, changes in P_{CENT} will be smaller than S by a factor of 1 minus the ratio of precipitation at the edge of the tropical domain to that at location of maximum precipitation.

Because precipitation is non-zero on the edge of the tropical domain, one would expect S values to exceed P_{CENT} changes *if ΔP was well characterized by a meridional translation* of P_{PI} which is the opposite of what is seen in our results (Fig. 3A). Instead, our results suggest that S values are less than changes in P_{CENT} because the ΔP changes are so poorly described by meridional translations of the climatological precipitation. Instead, the P_{CENT} changes primarily reflect opposing changes in the amplitude of the NH and SH tropical precipitation peaks (e.g. ΔP under freshwater hosing in Fig. 2B) as was recently demonstrated by Adam (2021). Such opposing changes in the NH and SH precipitation peaks strongly impact P_{CENT} but only weakly project on to S . We note the magnitude of S is also smaller than the precipitation power-weighted latitude (by a factor of 6 when using a power weighting of $N = 10$, not shown) a metric that responds sensitively to the relative magnitude of the bi-modal tropical precipitation maxima (Adam et al. 2016b).

4 Summary and discussion

The shifting mode (S) of (annual and zonal mean) tropical precipitation changes (ΔP)—defined here as the optimal meridional translation of the unperturbed precipitation—is found to be relatively useless for characterizing simulated zonal mean precipitation changes under a myriad of anthropogenic and paleoclimatic forcings. In response to global scale warming and cooling associated with LGM boundary conditions and CO₂ quadrupling, the fraction of ΔP described by S ($FRAC_{SHIFT}$) is 4% and 2% respectively. Even in the cases of strong hemispherically-asymmetric forcings such as freshwater hosing and NH volcanic forcing where $FRAC_{SHIFT}$ exceeds $FRAC_{INT}$ and $FRAC_{CON}$, ΔP is poorly characterized by the shift mode ($FRAC_{SHIFT} = 19\%$ and 17% respectively). In these cases, ΔP is also poorly characterized by the optimal fit of all tropical precipitation modes considered here with only 25% and 31% of the total ΔP explained as compared to 59% for all other simulations. Hemispherically asymmetric tropical precipitation responses are best characterized by changes in the relative amplitude of the tropical precipitation peaks in the NH and SH. Adam (2021) demonstrated that common metrics of “ITCZ shifts” respond to tropical precipitation changes that are best characterized by changes in the relative amplitude of bi-modal tropical

precipitation peaks in the absence of changes in the location of the peaks. These precipitation changes warrant further study from a dynamics perspective and should be viewed as distinct from an ITCZ shift, in its most literal sense.

It is possible that our interpretation of the term “ITCZ shift” as a meridional translation of the climatological precipitation pattern is overly literal and is different from that intended by the paleoclimate and climate dynamics communities. However, our main point here is that a meridional dipole in the pattern of forced precipitation change is not necessarily indicative of (i.e. statistically well described by) a meridional shift of the climatological precipitation. We hope our work here motivates future studies to clarify the definition of an “ITCZ shift” and quantify how consistent tropical precipitation changes are with the definition used. The various metrics used in literature to quantify “ITCZ shifts” should be renamed to more accurately represent the patterns of forced precipitation changes and the underlying links to the changes in the Hadley circulation that the metrics respond to.

We find that the magnitude of ITCZ shifts quantified by the optimal shift (S) method are generally small—less than 1° latitude in magnitude with the exception of the highly hemispherically asymmetric North Atlantic freshwater forcing (where $|S|$ ranges from 0.4° to 1.7° in response to 1 Sv freshwater hosing). S calculated from the simulated precipitation response to forcing is smaller (by approximately one half) than that inferred using alternative statistical metrics of “ITCZ shifts” such as P_{CENT} (Frierson and Hwang 2012; Donohoe et al. 2013) and the precipitation power weighted latitude (Adam et al. 2016a).

The magnitude of optimal shifts (S) diagnosed in this study provide additional support for the notion that zonal mean ITCZ shifts of more than a couple degrees latitude are not realized in forced model simulations. Small magnitude ITCZ shifts have also been deduced from paleoclimate proxy sea surface temperature (SST) reconstructions during the LGM, mid-Holocene and across Heinrich events using statistical relationships between the inter-hemispheric SST gradient and the zonal mean ITCZ location derived from modern day observed variability and forced simulations (McGee et al. 2014). Compilations of paleo hydrological proxy records throughout the tropics meanwhile have been interpreted as representing larger magnitude ($> 5^\circ$) regional shifts of the ITCZ during the LGM and Little Ice Age (Arbuszewski et al. 2013; Pahnke et al. 2007; Haug et al. 2001; Sachs et al. 2009). Simulated ITCZ shifts in response to paleoclimate forcing are highly zonally inhomogeneous (Atwood et al. 2020). Together, these results suggest that sparse compilations of proxy records likely can only inform on regional (as opposed to zonal mean) shifts of the ITCZ. Our work here further suggests that, even if we had reliable proxy records for reconstructing *zonal mean precipitation*,

such changes should not be interpreted solely in terms of a meridional translation of the climatological precipitation given the small fraction of simulated ΔP explained by the shift mode relative to the intensity and contraction modes. Indeed, model simulations suggest that a decrease (increase) in precipitation proportional to the mean state precipitation throughout the tropics in response to global mean cooling (warming) is a good zeroth order hypothesis and has slightly more explanatory power for explaining the spatial structure of tropical hydrological changes than the thermodynamic constraints on (P–E) changes advanced by Held and Soden (2006) as discussed in Sect. 3.2.

A zonal mean ITCZ shift of 3° (as measured by changes in P_{CENT}) requires a sustained hemispheric asymmetry of atmospheric heating equivalent to a simultaneous doubling of CO_2 in one hemisphere and CO_2 halving in the opposing hemisphere (resulting in 1 PW of atmospheric energy transport across the equator) assuming no radiative feedbacks (which generally damp localized forcing Donohoe and Voigt 2015). We cannot comprehend a forcing that could achieve a hemispheric asymmetry in atmospheric heating of the magnitude necessary to shift the ITCZ by more than a couple of degrees—even more so when the damping impact of ocean circulation anomalies is considered (Green et al. 2019). The preponderance of modeling, theoretical and empirical observational evidence suggests that large magnitude ($> 3^\circ$) zonal mean ITCZ shifts under paleoclimate forcing are dynamically unrealistic and are unlikely to explain the spatial structure of tropical precipitation changes.

We find that contractions and intensifications of the tropical precipitation respond robustly and in unison (with fixed scaling) to external forcing: e.g. tropical precipitation intensifies and meridionally contracts under global warming, and reduces and meridionally expands under global cooling. The tight (empirically derived) scaling between contractions and intensifications allow us to define a joint contracting and intensifying mode (CI) mode of tropical precipitation that efficiently describes the majority of the tropical precipitation changes under LGM and $4\times\text{CO}_2$ forcing.

What mechanism accounts for the tight coupling between contraction and intensification seen across the ensemble of forcing experiments (Fig. 3B)? The meridional contraction of tropical precipitation in response to global warming under anthropogenic forcing has been noted in several studies (Lau and Kim 2015; Su et al. 2017). The proposed mechanisms of precipitation contraction under warming include: (1) changes in the efficiency of transient-eddy energy and moisture fluxes (Byrne and Schneider 2016a; Nolan et al. 2010; Peters et al. 2008), (2) cloud radiative effects (Su et al. 2017), and (3) increased gross moist stability (GMS) of the tropics under warming that impacts the meridional width of convective regions (Chou et al. 2009; Byrne and Schneider 2016b). Donohoe et al. (2019) found that a contraction

of annual mean precipitation resulted from a reduced seasonal migration of the ITCZ off the equator under global warming and argued that the latter resulted from enhanced GMS of the tropical atmosphere. Adam et al. (2016b) found the models with more meridionally contracted mean state tropical precipitation had enhanced net energy input into the tropical atmosphere which is consistent with enhanced GMS leading to contraction of tropical precipitation. All of these mechanisms would be expected to lead to an expansion of tropical precipitation under global cooling in addition to the contraction seen under global warming as found in the present study. However, it is unclear whether the degree of simulated contraction is controlled by the magnitude of tropical surface warming, the GMS change, the degree of precipitation intensification (which would be consistent with our results in Fig. 3B), and/or by changes in seasonality. In future work, we hope to apply the optimal characterization of ΔP to seasonal precipitation changes to disentangle these proposed mechanisms by asking whether annual mean contractions result from contractions during all seasons or, alternatively, reflect seasonal precipitation shifts during the solstitial seasons that rectify to an annual contraction. Given the strong seasonality of zonal mean tropical precipitation, we also plan to examine whether the large fraction of ΔP explained by the *CI* extends to seasonal precipitation changes or, rather, the annual mean changes reflect more subtle changes in the seasonality of precipitation.

How can our findings here be used to interpret large-scale patterns of past tropical precipitation changes based on compilations of sparsely located paleoproxy hydroclimate records? One possible path forward is to shift, contract and intensify the observed climatological precipitation pattern (Xie and Arkin 1996) to optimally fit (i.e. minimize the RMS mismatch) the discrete proxy data. If we can trust the scaling between the contraction and intensification scalars found across the ensemble of climate model simulations (Fig. 3B), then we can reduce the number of free parameters in the optimal fit to two (the shift and *CI* mode), thus, improving statistical significance of the fit to proxy data. This procedure would allow the optimal shift and *CI* mode change to be quantified in past climates. In addition, the low explanatory power of the shifting mode motivates the search for an alternative mode (and underlying dynamics) that captures changes in the relative magnitude of the bi-modal precipitation peaks as discussed by Adam (2021).

Our work here has focused exclusively on zonal and annual mean tropical precipitation changes whereas the simulated tropical precipitation response has been shown to feature strong zonal inhomogeneities (Braconnot et al. 2007a, 2012) with robust zonally localized responses to forcing (Atwood et al. 2020). We plan to extend our optimal shifting, intensifying and contracting framework to a two-dimensional framework to characterize zonal asymmetries

in the precipitation response to forcing in order to better understand and relate mechanisms of regional precipitation changes to compilations of proxy records.

Acknowledgements All CMIP3 and CMIP5 climate model data were downloaded from the Earth System Grid Federation (ESGF) node hosted by Lawrence Livermore National Laboratory. AD and ARA were funded by the National Science Foundation Paleo Perspective on Climate Change (P2C2) Grant number AGS-1702827.

Author contributions AD formulated the optimization procedure, analyzed the model simulations and wrote the manuscript. ARA designed and ran the freshwater hosing experiments, compiled model simulations and edited the manuscript. DSB provided feedback on model design, edited manuscript and provided feedback on **which colors (shades of pink) readers find generally offensive in graphics**.

Funding AD and ARA were funded by the National Science Foundation Paleo Perspective on Climate Change (P2C2) Grant number AGS-1702827.

Data and material availability The model precipitation data used in this study were uploaded to Figshare and published with the following doi (10.6084/m9.figshare.12284282). All CMIP5/PMIP3 and CMIP3/PMIP2 climate model data were downloaded from the Earth System Grid Federation (ESGF) node hosted by Lawrence Livermore National Laboratory data repositories (<https://esgf-node.llnl.gov/>).

Code availability Not applicable.

Declarations

Conflict of interest All authors declare that they have no competing interests.

References

- Adam O (2021) Dynamic and energetic constraints on the modality and position of the intertropical convergence zone in an aquaplanet. *J Clim* 34(2):527–543
- Adam O, Bischoff T, Schneider T (2016) Seasonal and interannual variations of the energy flux equator and ITCZ. Part I: Zonally averaged ITCZ position. *J Clim* 29(9):3219–3230
- Adam O, Schneider T, Brient F, Bischoff T (2016) Relation of the double-ITCZ bias to the atmospheric energy budget in climate models. *Geophys Res Lett*. <https://doi.org/10.1002/2016GL069465>
- Arbuszewski JA, deMenocal PB, Cleroux C, Bradtmiller L, Mix A (2013) Meridional shifts of the Atlantic Intertropical Convergence Zone since the Last Glacial Maximum. *J Atmos Sci* 6:959–962
- Atwood AR, Donohoe A, Battisti DS, Liu X, Pausata F (2020) Robust longitudinally variable response of the ITCZ to a myriad of climate forcings. *Geophys Res Lett* 20:e2020GL088833
- Baldwin JW, Atwood A, Vecchi G, Battisti DS (2021) Outsize influence of Central American orography on global climate. *AGU Adv* 20:2. <https://doi.org/10.1029/2020AV000343>
- Berger AL (1978) Long-term variations of caloric insolation resulting from Earth's orbital element. *Quatern Res* 9:139–167

- Bird BW, Abbott MB, Rodbell DT, Vuille M (2011) Holocene tropical South American hydroclimate revealed from a decadal resolved lake sediment $\delta O-18$ record. *Earth Planet Sci Lett* 310:192–202
- Braconnot P, Otto-Bliesner B, Harrison S, Joussaume S, Peterschmitt JY, Abe-Ouchi A, Crucifix M, Driesschaert E, Fichefet T, Hewitt CD, Kageyama M, Kitoh A, Lañé A, Loutre MF, Marti O, Merkel U, Ramstein G, Valdes P, Weber SL, Yu Y, Zhao Y (2007a) Results of PMIP2 coupled simulations of the Mid-Holocene and Last Glacial Maximum. Part 1: Experiments and large-scale features. *Clim Past Discuss* 20:261–277
- Braconnot P, Otto-Bliesner B, Harrison S, Joussaume S, Peterschmitt JY, Abe-Ouchi A, Crucifix M, Driesschaert E, Fichefet T, Hewitt CD, Kageyama M, Kitoh A, Lañé A, Loutre MF, Marti O, Merkel U, Ramstein G, Valdes P, Weber SL, Yu Y, Zhao Y (2007b) Results of PMIP2 coupled simulations of the Mid-Holocene and Last Glacial Maximum. Part 2: Feedbacks with emphasis on the location of the ITCZ and mid- and high latitudes heat budget. *Clim Past Discuss* 20:279–296
- Braconnot P, Harrison S, Kageyama M, Bartlein PJ, Masson-Delmotte V, Abe-Ouchi A, Otto-Bliesner B, Zhao Y (2012) Evaluation of climate models using paleoclimatic data. *Nat Clim Chang* 2(6):417–424
- Byrne MP, Schneider T (2016) Energetic constraints on the width of the Intertropical Convergence Zone. *J Clim* 29:4709–4721
- Byrne MP, Schneider T (2016) Narrowing of the ITCZ in a warming climate: physical mechanisms. *Geophys Res Lett* 43:11350–11357
- Chiang JCH, Bitz CM (2005) The influence of high latitude ice on the position of the marine intertropical convergence zone. *Clim Dyn*. <https://doi.org/10.1007/s00382-005-0040-5>
- Chou MD, Neelin J, Chen C, Tu J (2009) Evaluating the “rich-get-richer” mechanism in tropical precipitation change under global warming. *J Clim* 22:1982–2005
- Colose C, Legrande A, Vuille M (2016) Hemispherically asymmetric volcanic forcing of tropical hydroclimate during the last millennium. *Earth Syst Dyn* 7:681–696
- Donohoe A, Voigt A (2015) Why future shifts in tropical precipitation will likely be small: the location of the tropical rain belt and the hemispheric contrast of energy input to the atmosphere. In: Wang S, Yoon J, Gillies R (eds) *Patterns of climate extremes; trends and mechanisms*. American Geophysical Union Books, Funk
- Donohoe A, Marshall J, Ferreira D, McGee D (2013) The relationship between ITCZ location and atmospheric heat transport across the equator: from the seasonal cycle to the Last Glacial Maximum. *J Clim* 26(11):3597–3618
- Donohoe A, Atwood AR, Byrne MP (2019) Controls on the width of tropical precipitation and its contraction under global warming. *Geophys Res Lett* 46:9958–9967. <https://doi.org/10.1029/2019GL082969>
- Frierson DMW, Hwang YT (2012) Extratropical influence on ITCZ shifts in slab ocean simulations of global warming. *J Clim* 25:720–733
- Green B, Marshall J, Campin JM (2019) The sticky ITCZ: ocean-modulated ITCZ shifts. *Clim Dyn* 53:1–19. <https://doi.org/10.1007/s00382-019-04623-5>
- Haug GH, Hughen KA, Sigman DM, Peterson LC, Rohl U (2001) Southward migration of the intertropical convergence zone through the Holocene. *Science* 293:1304–1308
- Held I, Soden B (2006) Robust responses of the hydrological cycle to global warming. *J Adv Model Earth Syst* 19(21):5686–5699
- Hwang YT, Frierson DMW, Kang SM (2013) Anthropogenic sulfate aerosol and the southward shift of tropical precipitation in the late 20th century. *Geophys Res Lett* 40(11):2845–2850
- Jacobel AW, McManus JF, Anderson RF, Winckler G (2016) Large deglacial shifts of the Pacific Intertropical Convergence Zone. *Commun Nat*. <https://doi.org/10.1038/ncomms10449>
- ...Kageyama M, Braconnot P, Harrison S, Haywood A, Jungclauss J, Otto-Bliesner B, Peterschmitt J, Abe-Ouchi A, Albani S, Bartlein P, Brierley C, Crucifix M, Dolan A, Fernandez-Donado L, Fischer H, Hopcroft P, Ivanovic R, Lambert F, Lunt D, Mahowald N, Peltier W, Phipps S, Roche D, Schmidt G, Tarasov L, Valdes P, Zhang Q, Zhou T (2018) The PMIP4 contribution to CMIP6. Part 1: Overview and over-arching analysis plan. *Geosci Model Dev* 11:1033–1057. <https://doi.org/10.5194/gmd-11-1033-2018>
- Kang SM (2020) Extratropical influence on the tropical rainfall distribution. *Curr Clim Change Rep* 6:24–36
- Kang SM, Held IM, Frierson DMW, Zhao M (2008) The response of the ITCZ to extratropical thermal forcing: idealized slab-ocean experiments with a GCM. *J Clim* 21:3521–3532
- Koutavas A, Lynch-Stieglitz J (2004) Variability of the marine ITCZ over the eastern Pacific during the past 30,000 years. In: Diaz HF, Bradley RS (eds) *The Hadley circulation: present, past and future*. Springer, Berlin, pp 347–369
- Lau W, Kim K (2015) Robust Hadley circulation changes and increasing global dryness due to CO₂ warming from CMIP5 model projections. *Proc Natl Acad Sci USA* 122:3630–3635
- Liu X, Battisti DS, Donohoe A (2018) Tropical precipitation and cross-equatorial ocean heat transport during the mid-Holocene. *J Clim* 30(10):3529–3547
- McGee D, Donohoe A, Marshall J, Ferreira D (2014) Changes in tropical precipitation, ITCZ location and hemispheric energy budgets at the Last Glacial Maximum, Heinrich Stadial 1, and the mid-Holocene. *Earth Planet Sci Lett* 390:69–79
- Nolan DS, Powell SW, Zhang C, Mapes BE (2010) Idealized simulations of the intertropical convergence zone and its multilevel flows. *J Atmos Sci* 67:4028–4053
- Pahnke K, Sachs JP, Keigwin L, Timmerman A, Xie SP (2007) Eastern tropical pacific hydrologic changes during the past 27,000 years from D/H ratios in alkenones. *Paleoceanography*. <https://doi.org/10.1029/2007PA001>
- Pausata FSR, Chafik L, Caballero R, Battisti DS (2015a) Impacts of high-latitude volcanic eruptions on ENSO and AMOC. *Proc Natl Acad Sci USA* 112(45):13784–13788
- Pausata FSR, Grini A, Caballero R, Hannachi A, Seland O (2015b) High-latitude volcanic eruptions in the Norwegian Earth system model: the effect of different initial conditions and of the ensemble size. *Tellus* 67(1):26728
- Peters ME, Kuang Z, Walker CC (2008) Analysis of atmospheric energy transport in ERA-40 and implications for simple models of the mean tropical circulation. *J Clim* 21:5229–5241
- Sachs JP, Sachse D, Smittenberg RH, Zhang Z, Battisti DS, Golubic S (2009) Southward movement of the Pacific intertropical convergence zone AD 1400–1850. *Nat Geol Sci* 2:519–525
- Sachs JP, Blois JL, McGee T, Wolhowe M, Haberle S, Clark G, Atahan P (2018) Southward shift of the Pacific ITCZ during the Holocene. *Paleoceanogr Paleoclimatol* 33(12):1383–1395
- Schneider T, Bischoff T, Haug GH (2014) Migrations and dynamics of the intertropical convergence zone. *Nature* 513:45–53
- Stevenson S, Otto-Bliesner B, Fasullo J, Brady E (2016) El Niño like hydroclimate responses to last millennium volcanic eruptions. *J Clim* 29(8):2907–2921
- Su H, Jiang JH, Neelin D, Shen J, Zhai C, Yue Q, Wang Z, Huang YCL, Stephens GL, Yung YL (2017) Tightening of tropical ascent and high clouds key to precipitation change in a warmer climate. *Nat Commun* 8(15):771
- Taylor KE, Stouffer RJ, Meehl GA (2012) An overview of CMIP5 and the experiment design. *Bull Am Meteorol Soc* 93:485–498
- Timmermann A, Okumura Y, An SI, Clement A, Dong B, Guilyardi E, Hu A, Jungclauss JH, Renold M, Stocker TF, Stouffer RJ, Sutton R, Xie SP, Yin J (2007) The influence of a weakening of

- the Atlantic meridional overturning circulation on ENSO. *J Clim* 20(19):4899–4919
- Wang YJ, Cheng H, Edwards RL, An ZS, Wu JY, Shen CC, Dorale JA (2001) A high-resolution absolute-dated late pleistocene monsoon record from Hulu cave, China. *Science* 294:2345–2348
- Wei HH, Bordoni S (2018) Energetic constraints on the ITCZ position in idealized simulations with a seasonal cycle. *J Adv Model Earth Syst* 10(7):1708–1725
- Xie P, Arkin PA (1996) Analyses of global monthly precipitation using gauge observations, satellite estimates, and numerical model predictions. *J Clim* 9:840–858
- Yan H, Wei W, Amd WS, An Z, Zhou W, Liu Z, Wang Y, Carter RM (2015) Dynamics of the intertropical convergence zone over the western Pacific during the Little Ice Age. *Nat Geol Sci* 8:315–320
- Zhao B, Federov A (2020) The seesaw response of the intertropical and south pacific convergence zones to hemispherically asymmetric thermal forcing. *Clim Dyn* 54:1639–1653

Publisher's Note Springer Nature remains neutral with regard to jurisdictional claims in published maps and institutional affiliations.